A modular toolkit to inhibit proline-rich motif–mediated protein–protein interactions

Robert Opitz[a,1], Matthias Müller[a,1], Cédric Reuter[b,1], Matthias Barone[a,1], Arne Soicke[b], Yvette Roske[c], Kirill Piotukh[a], Peter Huy[b], Monika Beerbaum[a], Burkhard Wiesner[a], Michael Beyermann[a], Peter Schmieder[a], Christian Freund[d], Rudolf Volkmer[a], Hartmut Oschkinat[a], Hans-Günther Schmalz[b,2], and Ronald Kühne[a,2]

[a]Leibniz-Institut für Molekulare Pharmakologie, 13125 Berlin, Germany; [b]Department für Chemie, Universität zu Köln, 50939 Köln, Germany; [c]Max Delbrück Centrum für Molekulare Medizin, 13125 Berlin, Germany; and [d]Institut für Chemie und Biochemie, Freie Universität Berlin, 14195 Berlin, Germany

Edited by Samuel H. Gellman, University of Wisconsin–Madison, Madison, WI, and approved March 6, 2015 (received for review November 18, 2014)

Small-molecule competitors of protein–protein interactions are urgently needed for functional analysis of large-scale genomics and proteomics data. Particularly abundant, yet so far undruggable, targets include domains specialized in recognizing proline-rich segments, including Src-homology 3 (SH3), WW, GYF, and *Drosophila* enabled (Ena)/vasodilator-stimulated phosphoprotein (VASP) homology 1 (EVH1) domains. Here, we present a modular strategy to obtain an extendable toolkit of chemical fragments (ProMs) designed to replace pairs of conserved prolines in recognition motifs. As proof-of-principle, we developed a small, selective, peptidomimetic inhibitor of Ena/VASP EVH1 domain interactions. Highly invasive MDA MB 231 breast-cancer cells treated with this ligand showed displacement of VASP from focal adhesions, as well as from the front of lamellipodia, and strongly reduced cell invasion. General applicability of our strategy is illustrated by the design of an ErbB4-derived ligand containing two ProM-1 fragments, targeting the yes-associated protein 1 (YAP1)-WW domain with a fivefold higher affinity.

Ena | VASP | protein–protein interaction | actin cytoskeleton | cell migration

Proline-rich segments (PRSs) belong to the most abundant sequence motifs of the proteome (1), interacting frequently with PRS-recognizing domains (PRDs), such as EVH1, SH3, GYF, and WW. Although exhibiting different tertiary structures, PRDs expose clusters of aromatic residues, forming a shallow, corrugated binding groove with a hydrogen bond-donating residue (W, Y) in the central position. In the bound state, PRSs often show a conformation closely related to the ideal left-handed polyproline II (PPII) helix characterized by backbone angles of $\Phi = -78°$ and $\Psi = +146°$ (2). As a consequence of the axial symmetry of PPII helices, two different types of consensus motifs occur: one containing PxxP specifically recognized by the EVH1 and SH3 domains, the other comprising xPPx, typical for motifs binding at WW and GYF domains. The conserved prolines represent the core of the consensus motifs and interact intimately with the exposed aromatic side chains. They cannot be replaced by any other natural amino acid without complete loss of affinity (2, 3). On the other hand, the core motif alone binds only very weakly to its PRD. Further interactions of flanking residues located outside the core motif contribute substantially to both affinity and specificity. Incorporation of nonnatural amino acids in place of such specificity-determining residues is therefore often beneficial for binding (4–9). However, peptide ligands display a number of disadvantages when used as competitors, among them metabolic instability and often low cell permeability. Cell-permeable small molecules that grant the ability to modulate the function of PRDs are still not available.

Here, we present a modular concept for the systematic development of such low-molecular weight compounds. It is based on molecular building blocks that can replace the conserved prolines within the core motif without any loss of affinity. Combinations of such building blocks allow complete replacement of the proline-rich core motifs. They may be supplemented with organic scaffolds addressing the flanking epitopes to obtain peptidomimetic inhibitors of PRDs, highly desirable for functional analysis of PRS-mediated protein–protein interactions.

As proof of concept, we developed a peptidomimetic inhibitor targeting the enabled/vasodilator-stimulated phosphoprotein (Ena/VASP) family Ena/VASP homology 1 (EVH1) domains. This protein family is involved in modulation of the actin cytoskeleton, a complex and highly regulated process, which is the driving force of directed cell migration (10, 11) and plays important roles in disease-relevant processes like tumor metastasis (12, 13). The Ena/VASP family proteins [i.e., VASP, enabled homolog (EnaH), and Ena-VASP–like (EVL) (14–16)] are notably localized at focal adhesions and lamellipodia. Single Ena/VASP protein deletions are mostly compensated for the other members of the family (17); however, triple knock-out mice are embryonic lethal (18, 19). The proteins comprise EVH1 and Ena/VASP homology 2 (EVH2) domains, separated by a proline-rich region. Although EVH2 binds to the barbed ends of actin filaments, EVH1 interacts with proteins, like zyxin or lamellipodin (Lpd also called RAPH1), that contain the class 1 EVH1 consensus motif [FYWL]P.ϕP (ϕ is an aliphatic amino acid) (2, 20–22). Using our peptidomimetic inhibitor, we show that inhibition of the Ena/VASP

Significance

Protein–protein interactions mediated by proline-rich motifs are involved in regulation of many important signaling cascades. Protein domains specialized in recognition of these motifs expose a flat and relatively rigid binding site that preferentially interacts with sequences adopting a left-handed polyproline helix II. Here, we present a toolkit of new chemical entities that enables rational construction of selective small-molecule inhibitors for these protein domains. As proof of principle, we developed a selective, cell-permeable inhibitor of *Drosophila* enabled (Ena)/vasodilator-stimulated phosphoprotein (VASP) homology 1 (EVH1) domains of the Ena/VASP protein family. Invasive breast-cancer cells treated with our EVH1 inhibitor showed strongly reduced cell invasion.

Author contributions: H.-G.S. and R.K. designed research; R.O., M.M., C.R., M. Barone, and A.S. performed research; Y.R., K.P., P.H., M. Beerbaum, B.W., M. Beyermann, C.F., and R.V. contributed new reagents/analytic tools; R.O., M.M., C.R., M. Barone, A.S., Y.R., K.P., P.H., M. Beerbaum, B.W., M. Beyermann, P.S., R.V., H.O., H.-G.S., and R.K. analyzed data; and H.O., H.-G.S., and R.K. wrote the paper.

The authors declare no conflict of interest.

This article is a PNAS Direct Submission.

Freely available online through the PNAS open access option.

Data deposition: The atomic coordinates and structure factors have been deposited in the Protein Data Bank, www.pdb.org (PDB ID code 4MY6).

[1]R.O., M.M., C.R., and M. Barone contributed equally to this work.

[2]To whom correspondence may be addressed. Email: schmalz@uni-koeln.de or kuehne@fmp-berlin.de.

This article contains supporting information online at www.pnas.org/lookup/suppl/doi:10.1073/pnas.1422054112/-/DCSupplemental.

family EVH1 domains strongly influences both cellular localization of VASP as well as cell migration.

Results

Design and Synthesis of ProM Building Blocks. We designed a novel class of conformationally restricted small-molecule fragments that should result in nonhydrolyzable yet cell-permeable, peptidomimetic small-molecule interaction inhibitors of PRDs. These molecules, coined ProM-1, ProM-2, ProM-3, and ProM-4, maintain a carbonyl functionality within a rigidified, nonaromatic scaffold and were aimed to substitute the strictly conserved prolines within PRS consensus motifs. In this small but extendable toolkit of fragments, the scaffolds ProM-1 and ProM-2 replace a diproline motif in PPII conformation whereas ProM-3 and ProM-4 substitute for an xP motif (Fig. 1*A*). Their frameworks show subtle conformational differences to satisfy individual steric requirements for a particular binding site. Similar to the foldamer concept (23), appropriate combinations of ProMs allow optimal complementarity of hydrophobic interactions between the domain surface and the ligand to be achieved. In a previously published pilot study, we showed that ProM-1 was able to replace a diproline motif in a peptide recognized by Fyn-SH3 whereas the respective, complete PxxP recognition motif could not be replaced using a combination of this building block (24).

The new fragments were stereoselectively synthesized in Fmoc-protected form (Fig. 1*B*; see *SI Appendix* for characterization of ProMs). The modular strategy relies on the coupling of building blocks **B1** to **B4** with enantiopure *cis*- or *trans-tert*-butyl 5-vinylprolinate (c/t5VP) (25), cyclization of the resulting dipeptides (**DP1** to **DP4**) through Ru-catalyzed ring closing metathesis (26), and final replacement of the Boc-protecting group by Fmoc (Fig. 1*B*). The preparation of the required building blocks was achieved on a multigram scale by exploiting, as a key step, either the Cu-catalyzed 1,4-addition of vinyl-MgBr to a cyclic dehydro-amino acid derivative (**A1** and **A4**, respectively) (27), diastereoselective vinylation (formylation/ methylenation) of the protected proline **A2** (28), or the enantioselective Claisen rearrangement of the glycine derivative **A3** (29). The Fmoc-protected ProMs can subsequently be used for ligand synthesis, exploiting established protocols for peptide coupling.

Development of an Ena/VASP EVH1 Inhibitor. Starting from peptide **1**—derived from a segment of the surface protein ActA of *Listeria monocytogenes* that captures Ena/VASP proteins of the host cell via their EVH1 domains—we replaced stepwise its conserved sequence motif FPPPP (Fig. 2*A*). In the course of this work, dissociation constants were determined by both isothermal titration calorimetry (ITC) and fluorescence titration (FT). Computational inspection of the binding site suggested introduction of a hydrophobic substituent at the ortho position of the phenylalanine ring within the core motif. The largest gain in affinity of all tested unnatural amino acids was observed for 2-chloro-*L*-phenylalanine (2-Cl-F) (Fig. 2*A* and *SI Appendix*, Fig. S11 and Table S2). Replacement of the second pair of prolines within the FPPPP motif in **1** by ProM-1 or ProM-3 indicated preference for ProM-1, with its five-membered ring next to R1 (K_d = 0.8 μM) (Fig. 1*A* and *SI Appendix*, Tables S3 and S4). Additional replacement of the first pair of prolines by ProM-2, which was found to satisfy the specific steric requirements at this interaction site, yielded compound **2**, with the highest affinity to Ena/VASP EVH1 domains (K_d ranging from 0.2 to 0.6 μM) (Table 1). Reduction of **2** to the core motif led to the ligand Ac-[2-Cl-F]-[ProM-2]-[ProM-1]-OH (**4a**). Analogous to the testing of ProM-3

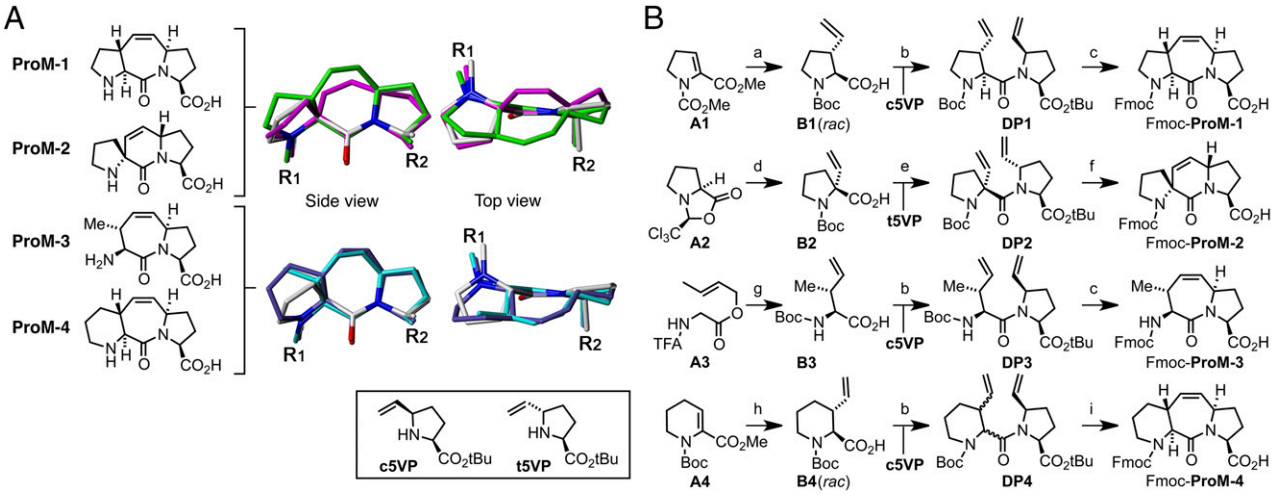

Fig. 1. Design and synthesis of the PPII helix-mimetic fragments. (*A*) A simple vinylidene bridge between positions 3 and 5 (ProM-1) or between positions 2 and 5 (ProM-2) of two adjacent prolines restricts the relative orientations of the pyrrolidine rings. The overlay of the X-ray structures of ProM-1 (green), ProM-2 (magenta), and a diproline motif in an ideal left-handed PPII helix conformation (white) shows that both tricyclic scaffolds present the pyrrolidine rings in a similar position relative to the dipeptide whereas the orientation of the vinylidene bridges differs. A formal N-terminal "ring opening" (ProM-3, cyan) or "ring extension" (ProM-4, blue) expands the portfolio of PPII-mimic modules while maintaining the orientation of the vinylidene bridge as found in ProM-1. The spatial positions (and exit vectors) of the R_1 and R_2 substituents are identical for all four structures. (*B*) Modular synthesis of ProM-1 to -4 in Fmoc-protected form. Reagents and conditions: (a) (*i*) vinyl-MgBr, CuBr·SMe_2 (30 mol%), THF, −30 °C, 3 h; (*ii*) TMSI (2 equiv.), CH_2Cl_2, reflux, 3 h; (*iii*) LiOH, H_2O/MeOH/THF (1:1:3), 20 °C, 12 h; iv. AcOH, Boc_2O, 3 d; 50% over four steps; see ref. 25; (b) PyBop, DIPEA, MeCN, 0 °C, 20 °C, 15 h, separation of diastereomers; for a standard protocol, see ref. 25; 42% (DP1), 75% (DP3); 42% (DP4); (c) (*i*) Grubbs II (10 mol%), CH_2Cl_2, reflux, 24 h; (*ii*) TFA, CH_2Cl_2, 0 °C, 20 °C, 1 h; (*iii*) Fmoc-Cl, $NaHCO_3$, H_2O/THF (2:1), 0 °C, 20 °C, 12 h; for a standard protocol, see ref. 25; 78% (Fmoc-ProM-1), 43% (Fmoc-ProM-3) over three steps; (d) (*i*) LiCl, LDA, HCO_2Me, THF, −78 °C, 30 min; (*ii*) H_2C = PPh_3, toluene, 80 °C, 2 h; (*iii*) AcCl (10 equiv), MeOH, 20 °C, 7 d; (*iv*) Boc_2O, DIPEA, CH_2Cl_2, 20 °C, 2.5 d; (*v*) LiOH, THF/MeOH/H_2O, 50 °C, 5 h; 41% over five steps; see ref. 28; (e) HATU (1.1 equiv.), DIPEA (1.98 equiv.), NMP, 85 °C, 24 h, 72%; (f) (*i*) Grubbs II (30 mol%), toluene, reflux, 15 h; (*ii*) (b) TFA, CH_2Cl_2, 20 °C, 1 h; (*iii*) Fmoc-Cl, $NaHCO_3$, H_2O/THF (2:1), 0 °C to rt, 15 h; 48% over three steps; (g) (*i*) $Al(OiPr)_3$ (1.1 equiv.), quinidine (2.5 equiv.), LiHMDS (5 equiv.), THF, −78 °C to rt, 15 h; (*ii*) NaOH, 1,3-dioxane/H_2O, rt, 15 h; then Boc_2O, rt, 15 h; 58% over two steps; see ref. 29; (h) (*i*) vinyl-MgBr, CuBr·SMe_2 (20 mol%), THF, −35 °C, 6 h, NH_4Cl (aq.), separation of diastereomers; (*ii*) LiOH, H_2O/MeOH/THF (1:1:3), 50 °C, 5 h, 28% over two steps; (i) (*i*) Grubbs-II (20 mol%), CH_2Cl_2, reflux, 48 h, separation of diastereomers; (*ii*) TFA, CH_2Cl_2, 0 °C, 20 °C, 1 h; (*iii*) Fmoc-Cl, $NaHCO_3$, H_2O/THF (2:1), 0 °C, 20 °C, 12 h, 34% over three steps; for a standard protocol, see ref. 25.

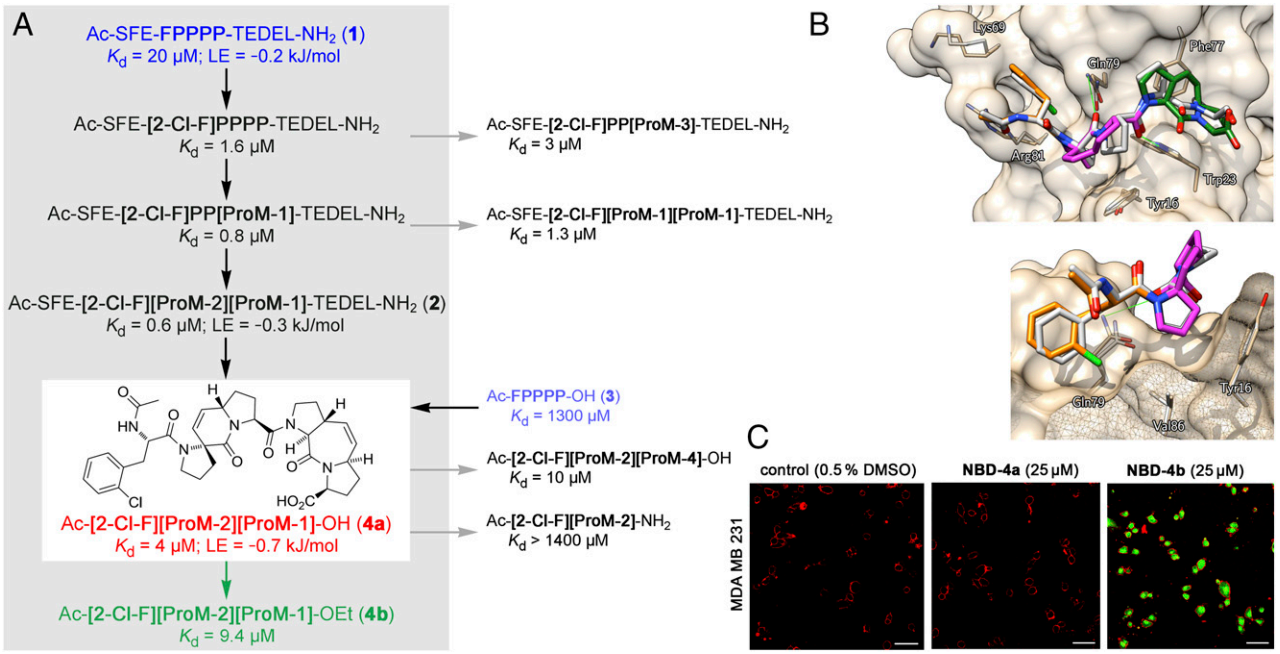

Fig. 2. Development of a low-molecular weight EVH1 inhibitor. (*A*) Schematic representation of compound optimization. Ligand efficiency (LE = ΔG°/number of heavy atoms) and affinity were improved by replacing the prolines by the PPII-mimetic modules and introducing 2-chloro-L-phenylalanine. Compound **4a** exhibits the highest LE. Esterfication yields the cell-permeable EVH1 inhibitor **4b**. All K_d values shown are measured using ITC. (*B*) X-ray structure (1.7 Å) of the EnaH- EVH1-domain in complex with **4a**. (*Upper*) Overlay of **4a** with the FPPPP motif of 1evh. The FPPPP motif-containing peptide (white) and **4a** (orange) exhibit the same binding mode (ProM-1, green; ProM-2, magenta). (*Lower*) Detailed view of the L-phenylalanine [1evh (31), white] binding pocket in comparison with bound 2-chloro-L-phenylalanine (orange). (*C*) Cell permeability of NBD-labeled **4a** and **4b**. NBD fluorescence is shown in green, and trypan blue stain (red) shows cell edges. Only **NBD-4b** yields significantly high NBD fluorescence in the cells. (Scale bars: 50 μm.)

described above, and again guided by structural considerations (acknowledging the fact that any aliphatic hydrophobic amino acid may be accommodated at the third proline position of the motif), we also tested ProM-4 (Fig. 1*A*), which contains a six-membered ring next to R1, as a replacement of the last two prolines. However, the compound containing ProM-4 was slightly less effective (Fig. 2*A* and *SI Appendix*, Table S5). Thus, the final 678-Da compound **4a** represents the best low-molecular weight inhibitor targeting all three Ena/VASP EVH1 domains addressed in this study. A substantial increase in affinity of at least 180-fold (EVL- and EnaH-EVH1) and 280-fold (VASP-EVH1) compared with the parent recognition sequence Ac-FPPPP-OH (**3**) was observed, caused by the introduction of only five additional heavy atoms (Table 1). Although the high affinity of our ligands substantially benefits from the chloro-substitution of F, the almost negligible affinity of the shortened ligand Ac-[2-Cl-F]-[ProM-2]-NH_2 in comparison with **4a** indicates the importance of retaining a certain ligand length covering the full FPPPP motif (Fig. 2 and *SI Appendix*, Table S5).

Esterification of 4a Yields Cell-Permeable Compound 4b. Sufficient cell permeabilities of the compounds are necessary to study their cellular activities. We found that the N-terminal 7-nitro-2,1,3-benzoxa-diazol-4-yl-labeled (NBD-) compounds **2** and **4a** were not able to penetrate the cell membrane. Assuming that the free carboxylic acid functions of **NBD-2** (total charge −4) and **NBD-4a** (total charge −1) are responsible for poor membrane permeability, we synthesized the corresponding NBD-labeled ethyl ester **NBD-4b**, whose cellular uptake was indicated by a significant increase in cytosolic fluorescence (Fig. 2*C* and *SI Appendix*, Fig. S29). HPLC analysis of **NBD-4b**–treated colorectal cancer HCT 116 cells exhibited a time-dependent increase of compound **NBD-4a** in the cells, indicating ester cleavage (*SI Appendix*, Fig. S30). Furthermore, when incubated with 150 μM unlabeled ester **4b** for 24 h, no significant loss of either HCT 116 or MDA MB 231 cell viability was observed (*SI Appendix*, Fig. S31).

Ligand 4a Selectively Inhibits Ena/VASP EVH1 Domains. Investigations concerning the selectivity of our ligands against different PRDs made us aware of the fact that the consensus motif of Ena/VASP EVH1 domains exhibits no overlap with those of other PRDs, apart from the occurrence of prolines (30). Therefore, we expected low cross-reactivity. Experimentally, we probed a possible cross-inhibition of other PRDs by NMR and ITC. In particular, the EVH1 class 2 domain of Homer1, which is most closely related to the Ena/VASP EVH1 class 1 domains, and the YAP1-WW, Fyn-SH3, and CD2BP2-GYF domains, as members of different PRD classes and containing the most similar PRSs, were analyzed (Table 2). Binding studies via ITC and ^{1}H-^{15}N-HSQC yielded large K_d values of around 400 μM and 330 μM for the interactions of **4a** with Homer EVH1 and YAP1-WW, respectively. Fyn-SH3

Table 1. K_d values (μM)of selected compounds

	Compound				
	1	**2**	**3**	**4a**	**4b**
VASP-EVH1					
$K_{d,FT}$	19(2)	0.28(0.09)	780(80)	2.7(0.7)	6.2(0.6)
$K_{d,ITC}$	22(1)	0.56(0.04)	1,300(400)	3.8(0.1)	9.4(0.5)
Enah-EVH1					
$K_{d,FT}$	10(3)	0.15(0.06)	460(70)	2.3(0.2)	4.1(0.3)
$K_{d,ITC}$	20(1)	0.34(0.03)	450(60)	2.4(0.1)	7.8(0.4)
EVL-EVH1					
$K_{d,FT}$	7(1)	0.19(0.05)	310(20)	1.4(0.2)	4.1(0.5)
$K_{d,ITC}$	10.4(0.4)	0.26(0.01)	700(300)	2.2(0.2)	5.8(0.7)

Values in parentheses represent SE.

Table 2. K_d values of 4a and selected compounds to representatives of other PRDs

	4a		PP-ligand		ProM-ligand	
Domain name	Consensus	K_d, μM	Sequence	K_d, μM	Sequence	K_d, μM
Fyn-SH3	*[RKY]..P..P*	5,900(900)	Ac-RAL**PP**LP-NH_2	18(5)	Ac-RAL**[ProM-1]**LP-NH_2	62(13)
YAP1-WW	*PP.Y*	330(60)	Ac-L**PPPP**YRHR-NH_2	21(2)	Ac-L**[ProM-1][ProM-1]**YRHR-NH_2	4.4(0.1)
Homer1-EVH1	*PP..F*	400(100)	Ac-ALT**PP**SPFRDS-NH_2	72(5)	Ac-ALT**[ProM-1]**SPFRDS-NH_2	800(100)
CD2BP2-GYF	*[QHR]{0.1}P[LP]PP[GS]H[RH]*	3,200(600)	Ac-EFGP**PP**GWLGR-NH_2	6.3(0.5)	Ac-EFGP**[ProM-1/2]**GWLGR-NH_2	N.D.

Consensus motifs of the domains are in italics. Prolines replaced by the ProM-fragments are in bold. N.D., not detectable.

and CD2BP2-GYF showed even weaker affinity (Table 2 and *SI Appendix*, Figs. S25–S28 and Table S7), clearly indicating a striking prevalence of **4a** to inhibit the Ena/VASP EVH1 domains.

The ProM-Toolkit Paves the Way to Develop Ligands also for Other PRD Families. To prove the potential of our current ProM toolkit and to test selectivity further, we developed new ligands exclusively addressing Homer1-EVH1, Fyn-SH3, YAP1-WW, and CD2BP2-GYF. Although for Fyn-SH3 the replacement of the diproline motif by ProM-1 resulted in a moderate loss of affinity, an almost fivefold higher affinity against YAP1-WW was observed with its ProM-modified ErbB4-derived ligand (Table 2, PP-ligand vs. ProM-ligand; and *SI Appendix*, Table S8). On the other hand, our ProM-toolkit was, so far, not suitable to substitute proline-rich motifs in peptides recognized by Homer1 EVH1 and CD2BP2-GYF (Table 2 and *SI Appendix*, Table S8). In this case, modeling studies based on available structures uncovered steric hindrances caused by the vinylidene bridges in the canonical binding mode.

X-Ray Structure of 4a in Complex with EnaH-EVH1 Verifies the Canonical Binding Mode. X-ray analysis of the EnaH-EVH1 domain in complex with compound **4a** (resolution 1.7 Å) (Fig. 2*B* and *SI Appendix*, Table S9 and Figs. S12–S16) confirmed the canonical binding mode (31), with the pyrrolidine rings of the two ProMs situated in the ligand-binding groove following the axis of the PPII helix. As expected, the complex is stabilized by two hydrogen bonds between (*i*) the oxygen of the carbonyl group bridging ProM-2 and ProM-1 and the Nε-H of Trp23 and (*ii*) the carbonyl oxygen of the seven-membered ring of ProM-2 and an Nε-H of Gln79. Furthermore, a third hydrogen bond is observed between the carbonyl oxygen of the N-terminal acetyl group and the Nη-H of Arg81. Moreover, the vinylidene bridge of the ProM-1 fragment interacts with Phe77. The 2-Cl-F moiety resides in the hydrophobic pocket surrounded by residues Lys69, Asn71, Gln79, Arg81, and Val86. The chlorine atom fills the additional space in the pocket between Gln79, Arg81, and Val86, thereby substantially improving binding efficiency (Fig. 2*B*). NMR studies of VASP- and EVL-EVH1 domains and **4a** confirmed similar binding modes (*SI Appendix*, Figs. S17–S20) for both interactions.

Ligands 2 and 4a Inhibit EVH1-Mediated Protein–Protein Interactions in Vitro. The potential of compounds **2** and **4a** to interfere with binding and localization of two well-known Ena/VASP EVH1 interaction partners—zyxin and Lpd—was investigated using the highly invasive breast-cancer cell line MDA MB 231 and the slow-migrating colorectal cancer cell line HCT 116, respectively. Zyxin is abundant in focal adhesions of both cell lines whereas Lpd localizes mainly at the leading edge of MDA MB 231 but could not be detected in HCT 116 cells. Lpd targets VASP via its proline-rich motifs to the lamellipodial tips, causing faster migration (32). Western blot analysis of pull-down experiments with immobilized glutathione-(S)-transferase (GST)-tagged EnaH-EVH1 or VASP-EVH1 applied to the cell lysates revealed zyxin in both cell lines as an EVH1 interaction partner whereas interactions with Lpd were detected only in MDA MB 231 cells (Fig. 3 and *SI Appendix*, Fig. S32). Both compounds displaced zyxin and Lpd from the GST-fusion proteins in a concentration-dependent manner and corresponding to their respective K_d values. Despite the high level of homology among the Ena/VASP family EVH1 domains, the EnaH and VASP constructs, but not the GST-EVL-EVH1 construct, pulled zyxin and Lpd, although at different amounts. Restricted accessibility of ligand-binding sites in the immobilized domains, the recruitment of other proteins, or additional contributions by flanking epitopes of the FPPPP motifs likely explain this behavior.

Inhibition of EVH1 Domains by 4b Reduces the Number of Stress Fibers and Inhibits Cell Invasion. To test cellular effects, we examined the response of both cell lines toward **4b**. Untreated HCT 116 cells showed distinctive F-actin in the form of stress fibers. Treatment with **4b** altered cell morphology: i.e., the number of cells exposing stress fibers was reduced by 50% (Fig. 4*A*, *Left*), and VASP is delocalized from focal adhesions, which are indicated by zyxin localization (Fig. 4*A*, *Right*).

Immunofluorescence staining of MDA MB 231 cells showed zyxin in focal adhesions and Lpd at the leading edge (Fig. 4*B*, columns 1 and 3, respectively). In both cases, these proteins colocalized with VASP (Fig. 4*B*, *Bottom*, columns 1 and 3). After treatment with **4b**, we detected a strongly reduced presence of VASP at both focal adhesions and at the leading edge (Fig. 4*B*, columns 2 and 4) whereas localization of zyxin and Lpd remained unaltered (Fig. 4*B*, *Top*, columns 2 and 4). MDA MB 231 cells treated with **4b** showed a remarkable two-thirds reduction of cell invasion, indicating the importance of EVH1 domain-dependent localization of VASP for this purpose (Fig. 4*C*). Due to the lack of Lpd in HCT 116, we only investigated interference of **4b** with the formation of focal adhesion complexes in this cell line.

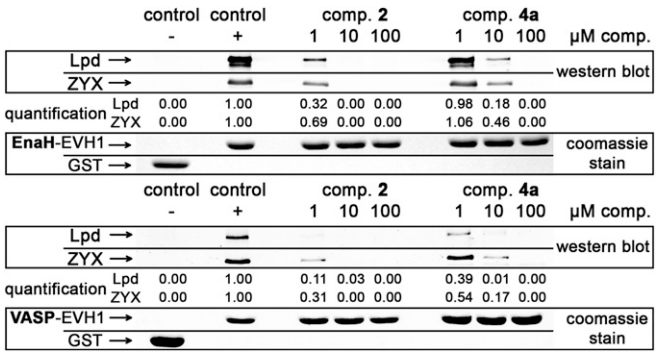

Fig. 3. Displacement of zyxin and Lpd from EnaH- and VASP-EVH1. Pull-down experiments with lysates from MDA MB 231 cells and GST-tagged EnaH-EVH1 (*Upper*) and VASP-EVH1 (*Lower*) immobilized on glutathione Sepharose beads (*Upper Frame*: Lpd and zyxin in Western blot analysis; *Lower Frame*: loading control). With GST alone, no zyxin/Lpd was pulled. GST-EVH1 pulled zyxin/Lpd. Zyxin/Lpd displacement from GST-EVH1 domains was performed by adding different concentrations of compounds **2** or **4a** to the lysate.

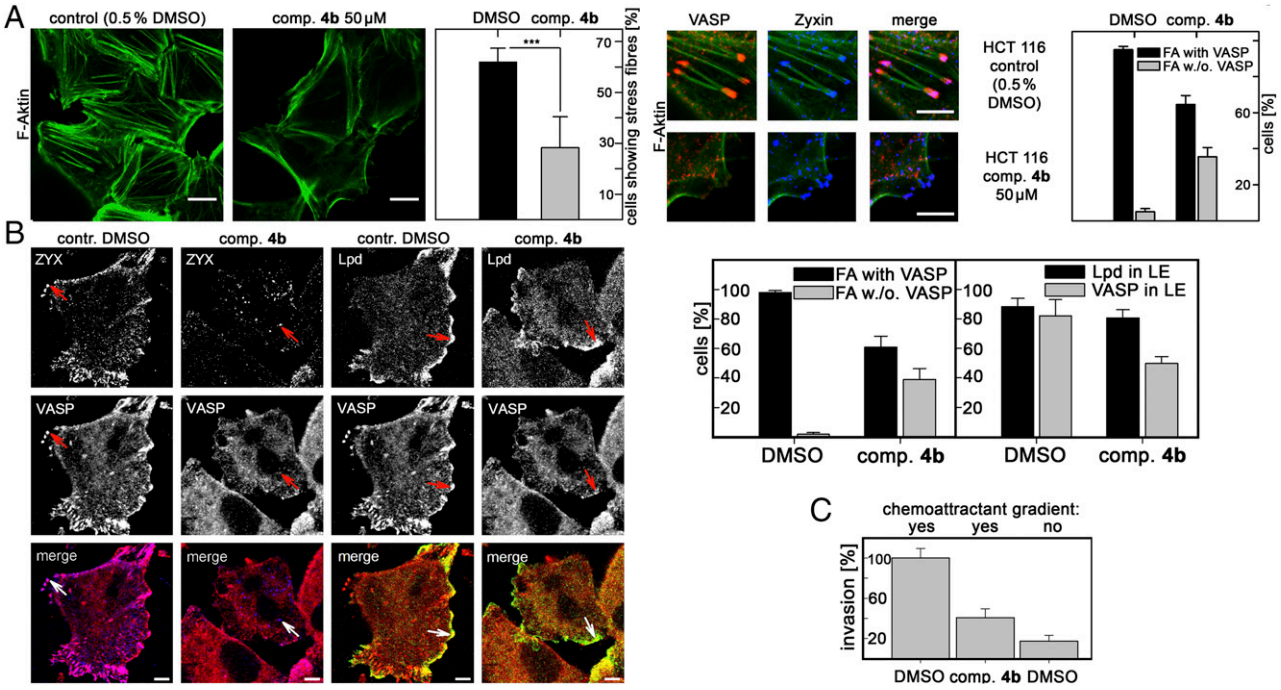

Fig. 4. Immunofluorescence and invasion assay. (*A*, *Left*) Stress-fiber (SF) formation of HCT 116 cells. Cells are stained for F-Actin. Control cells (*Left*) show SF. After treatment for 3 h with compound **4b**, the number of cells exhibiting SF was reduced by 50% (*Center*) (*SI Appendix*, Table S10). (Scale bars: 10 µm.) (*A*, *Right*) Immunofluorescent stain of HCT 116 cells (F-Actin, green; VASP, red; zyxin, blue; colocalization, purple). Control (*Upper* row, 0.5% DMSO) and compound **4b**-treated (*Lower* row) cells were incubated for 3 h. Control cells exhibit colocalization of VASP and zyxin in focal adhesions. Cells treated with **4b** showed zyxin in focal adhesions, but the colocalization with VASP was reduced by 30% (three replicates, $P < 0.001$, Pearson's χ^2 test) (*SI Appendix*, Table S11). (Scale bars: 10 µm.) (*B*, *Left*) Immunofluorescent stain of MDA MB 231. Control 0.5% DMSO (columns 1 and 3) and 100 µM compound **4b** (columns 2 and 4) incubated for 3 h. (*Top* row) zyxin (ZYX,) and Lpd; (*Middle* row) VASP; (*Lower* row) merge (ZYX, blue; VASP, red; colocal., purple; Lpd, green; colocal., yellow). (*B*, *Right*) Compound **4b**-treated cells showed a reduction of VASP location to focal adhesions (FAs) by ~40% and to the leading edge by 30% (*SI Appendix*, Tables S12 and S13). FAs are marked by zyxin, the leading edge by Lpd. The localization of zyxin and Lpd remains unchanged. (Scale bars: 5 µm.) (*C*) Matrigel invasion assay. MDA MB 231 cells invaded through a matrigel-coated 8-µm-pore membrane on (*i*) an FBS gradient (DMSO and compound **4b**) or (*ii*) in FBS without a gradient (DMSO) while incubating 100 µM **4b** for 14 h. The invaded cells on the lower side of the membrane were counted. The control (DMSO, with gradient) was set to 100%. Compound **4b** reduced the cell invasion by 64%.

Discussion

We synthesized a toolkit of four building blocks (ProM-1 to ProM-4) designed to replace the conserved PxxP and xPPx recognition motifs involved in PRS-mediated protein–protein interactions. As proof of concept, we developed a peptidomimetic, low-molecular weight inhibitor of the Ena/VASP family EVH1 domains that exhibits a fivefold higher affinity than the much larger ActA-derived peptide **1**. In comparison with the isolated recognition sequence Ac-FPPPP-OH (**3**), the affinity is increased at least by a factor of 180 (Fig. 2 and Table 1). Remarkably, this dramatic effect is caused by introduction of only five additional heavy atoms. The progress achieved becomes apparent by comparing ligand efficiencies (LE = ΔG°/number of heavy atoms) (33) of compounds **1**, **2**, and **4a**. The gain of LE from **1** (–0.2 kJ·mol^{-1}) over **2** (–0.3 kJ·mol^{-1}) to **4a** (–0.7 kJ·mol^{-1}) represents a considerable success because the average LE of drug candidates targeting protein–protein interfaces is about –1.0 kJ·mol^{-1} (34).

The X-ray structure of the EnaH-EVH1 domain in complex with **4a** indicates that ProMs mimic a PPII helix in the bound state, with the pyrrolidine rings of the ProMs perfectly matching the position of the conserved core motif prolines. The structural feature enhancing binding of **4a** to Ena/VASP EVH1 domains is the vinylidene bridge in the tricyclic system that, together with the specific flanking residue, also boosts specificity. Selectivity of **4a** is supported by improved PPII helix recognition in conjunction with optimized binding of flanking epitopes. Although the pure PPII helix recognition motif alone contributes little to affinity, it strongly affects the recognition, as indicated by the strong decrease in affinity detected for Ac-[2-Cl-F]-[ProM-2]-NH_2 (Fig. 2*A*).

Western blot analysis of Ena/VASP EVH1 pull-down experiments showed that **4a** is able to compete in a concentration-dependent manner with the focal adhesion protein zyxin, as well as with Lpd, a protein involved in directed cell migration and located at the front of lamellipodia. Although compound **4a** is poorly cell-permeable, the ester derivative **4b** can enter into cells, thereby allowing examination of its effect on cytoskeleton remodeling in cellular assays. Immunofluorescence staining of **4b**-treated colorectal cancer cells HCT 116 exhibits reduction of stress fibers and delocalization of VASP from focal adhesions. Keeping in mind that our ligands inhibit all three Ena/VASP family EVH1 domains, this result is supported by Furman et al. (18), who showed that the number of stress fibers is strongly reduced in primary endothelial mouse cells in which all three Ena/VASP proteins are knocked out. Cells treated with **4b** showed zyxin-rich spots indicating focal adhesions, but a strongly reduced presence of VASP in these locations. These findings correlate with the observation that cells with zyxin mutants lacking the FPPPP motif do not show colocalization of VASP (21), indicating that the loss of an Ena/VASP EVH1-mediated protein–protein interaction is responsible for reduction of stress fibers. Treatment of highly invasive MDA MB 231 breast-cancer cells with **4b** causes delocalization of VASP from the leading edge and from focal adhesions, thereby reducing strongly their ability for invasion. Hence, we suggest that EVH1-mediated protein–protein interactions play an important role in regulation of the dynamic remodeling of the actin cytoskeleton.

Compounds **4a** and its prodrug **4b** represent a successful proof of concept. To our knowledge, they are the first low-molecular weight inhibitors of Ena/VASP EVH1 domains. Compound **4b** thereby represents a novel chemical probe that allows examination into the complex role of this protein family in the regulation of cytoskeletal remodeling events.

Our ProM toolkit enables construction of specific inhibitors for both PxxP and xPPx recognizing domains as shown here for Ena/VASP EVH1 and YAP1-WW domains, respectively. Our results suggest the importance of flanking motifs outside the conserved prolines for specificity and affinity. Furthermore, the toolkit of ProM modules facilitates the fitting of the designed ligands in an optimal manner to the binding cavities. In the case of the YAP1-WW ligand, we identified a $[\text{ProM-1}]_2$ module as the optimal replacement of the conserved xPPx motif whereas, for the Ena/VASP EVH1 domains, a [ProM-2]-[ProM-1] motif was better suited. The sensitivity of the different ProMs toward small differences between the proline-binding sites represents an opportunity for the design of specific ligands. A gain of affinity by enhanced flanking epitope binding together with deselection against similar but nevertheless structurally distinct binding sites are the two critical factors that are likely to be exploited by our iterative approach of design, synthesis, and structure elucidation. The new inhibitors open new routes for pharmacological interference by directly modulating regulatory PRS-mediated protein–protein interactions in a specific manner.

Methods

Binding Studies. Dissociation constants were determined via FT and ITC. All experiments were done at 25 °C in 40 mM sodium phosphate, pH 7.3, 100 mM sodium chloride. For the Ena/VASP-EVH1 domains, the buffer additionally contained 1 mM DTT or 2 mM tris(2-carboxyethyl)phosphine (TCEP).

Crystallization. To freshly purified and concentrated protein, a 3:1 molar excess of ligand was added, and the solution was diluted with gel-filtration buffer to 15 mg/mL and incubated at 4 °C overnight. Crystals were grown by the sitting-drop vapor-diffusion method using 300 nL of protein mixture with an equal volume of well solution (2.2 M ammonium sulfate, 200 mM ammonium bromide) at 20 °C.

Pull-Down Assay. Pull-down experiments were performed by GST-tagged EnaH-EVH1, VASP-EVH1, and Evl-EVH1 immobilized on glutathione Sepharose 4B beads (GE) using lysates with a total protein concentration of 2.3 mg for HCT 116 and 1.5 mg for MDA MB 231, measured via ultraviolet/visible (UV/VIS) spectroscopy (1 Abs./mg, NanoDrop 1000; Thermo Scientific). Zyxin displacement was performed by adding different concentrations of compound **2** or **4a** to the lysate incubating overnight on beads at 4 °C. As a control, GST alone was immobilized to the beads and treated with lysate. The Western blot with target-specific antibody against zyxin [goat anti–zyxin pAb (1:1,000); scbt], Lpd [rabbit anti–Lpd pAb (1:1,000); scbt], and fluorescence of secondary antibody (IRDye 800; Licor) was measured on an infrared scanner (ODYSSEY; Licor). Loading controls are 1:20 dilutions in SDS/PAGE with Coomassie stain.

Migration Assay. The BD Matrigel invasion chamber 24-well plate (8.0 μm) cell-migration assay (BD Biosciences, Inc.) was performed as described in the manufacturer's guide. The experiments were done in triplicate with 50,000 cells (MDA MB 231) per well in (*i*) 10% (vol/vol) fetal serum bovine (FBS) gradient and (*ii*) 10% (vol/vol) FBS without a gradient. After 14 h of incubation with 100 μM compound **4b**—or 0.5% DMSO as a control—cells were fixed with p-formaldehyde and stained with crystal violet. The used microscope (Eclipse TS100; Nikon) had a 10/0.25 (air) objective (Nikon), and images were detected with a digital sight camera (Nikon). Five random fields per well were taken, and cells were counted with ImageJ (imagej.nih.gov/ij/; NIH).

All other methods and materials are described in *SI Appendix*.

ACKNOWLEDGMENTS. We thank Jenny Eichhorn for help with confocal microscopy, Bernhard Schmikale for support in peptide synthesis, Linda Ball for providing the GST-fused human VASP-EVH1 vector, Anne Diehl for allocating the human-lung cDNA library, and Maria J. Macias for providing the assignments for YAP1-WW, respectively. We acknowledge support from Deutsche Forschungsgemeinschaft Grants KU 845, SCHM 857, BE 1434, and SFB765.

1. Rubin GM, et al. (2000) Comparative genomics of the eukaryotes. *Science* 287(5461): 2204–2215.
2. Ball LJ, Kühne R, Schneider-Mergener J, Oschkinat H (2005) Recognition of proline-rich motifs by protein-protein-interaction domains. *Angew Chem Int Ed Engl* 44(19): 2852–2869.
3. Lim WA, Richards FM, Fox RO (1994) Structural determinants of peptide-binding orientation and of sequence specificity in SH3 domains. *Nature* 372(6504):375–379.
4. Ball LJ, et al. (2000) Dual epitope recognition by the VASP EVH1 domain modulates polyproline ligand specificity and binding affinity. *EMBO J* 19(18):4903–4914.
5. Zimmermann J, et al. (2003) Design of N-substituted peptomer ligands for EVH1 domains. *J Biol Chem* 278(38):36810–36818.
6. Golemi-Kotra D, et al. (2004) High affinity, paralog-specific recognition of the Mena EVH1 domain by a miniature protein. *J Am Chem Soc* 126(1):4–5.
7. Hunke C, Hirsch T, Eichler J (2006) Structure-based synthetic mimicry of discontinuous protein binding sites: Inhibitors of the interaction of Mena EVH1 domain with proline-rich ligands. *ChemBioChem* 7(8):1258–1264.
8. Link NM, Hunke C, Mueller JW, Eichler J, Bayer P (2009) The solution structure of pGolemi, a high affinity Mena EVH1 binding miniature protein, suggests explanations for paralog-specific binding to Ena/VASP homology (EVH) 1 domains. *Biol Chem* 390(5-6):417–426.
9. Holtzman JH, Woronowicz K, Golemi-Kotra D, Schepartz A (2007) Miniature protein ligands for EVH1 domains: Interplay between affinity, specificity, and cell motility. *Biochemistry* 46(47):13541–13553.
10. Le Clainche C, Carlier MF (2008) Regulation of actin assembly associated with protrusion and adhesion in cell migration. *Physiol Rev* 88(2):489–513.
11. Sadok A, Marshall CJ (2014) Rho GTPases: Masters of cell migration. *Small GTPases* 5:e29710.
12. Gertler F, Condeelis J (2011) Metastasis: Tumor cells becoming MENAcing. *Trends Cell Biol* 21(2):81–90.
13. Blanchoin L, Boujemaa-Paterski R, Sykes C, Plastino J (2014) Actin dynamics, architecture, and mechanics in cell motility. *Physiol Rev* 94(1):235–263.
14. Pollard TD, Cooper JA (2009) Actin, a central player in cell shape and movement. *Science* 326(5957):1208–1212.
15. Hu LD, Zou HF, Zhan SX, Cao KM (2008) EVL (Ena/VASP-like) expression is up-regulated in human breast cancer and its relative expression level is correlated with clinical stages. *Oncol Rep* 19(4):1015–1020.
16. Ferron F, Rebowski G, Lee SH, Dominguez R (2007) Structural basis for the recruitment of profilin-actin complexes during filament elongation by Ena/VASP. *EMBO J* 26(21): 4597–4606.
17. Hauser W, et al. (1999) Megakaryocyte hyperplasia and enhanced agonist-induced platelet activation in vasodilator-stimulated phosphoprotein knockout mice. *Proc Natl Acad Sci USA* 96(14):8120–8125.
18. Furman C, et al. (2007) Ena/VASP is required for endothelial barrier function in vivo. *J Cell Biol* 179(4):761–775.
19. Kwiatkowski AV, et al. (2007) Ena/VASP is required for neuritogenesis in the developing cortex. *Neuron* 56(3):441–455.
20. Bear JE, Gertler FB (2009) Ena/VASP: Towards resolving a pointed controversy at the barbed end. *J Cell Sci* 122(Pt 12):1947–1953.
21. Smith MA, et al. (2010) A zyxin-mediated mechanism for actin stress fiber maintenance and repair. *Dev Cell* 19(3):365–376.
22. Drees B, et al. (2000) Characterization of the interaction between zyxin and members of the Ena/vasodilator-stimulated phosphoprotein family of proteins. *J Biol Chem* 275(29):22503–22511.
23. Martinek TA, Fülöp F (2012) Peptidic foldamers: Ramping up diversity. *Chem Soc Rev* 41(2):687–702.
24. Zaminer J, et al. (2010) Addressing protein-protein interactions with small molecules: A Pro-Pro dipeptide mimic with a PPII helix conformation as a module for the synthesis of PRD-binding ligands. *Angew Chem Int Ed Engl* 49(39):7111–7115.
25. Reuter C, Huy P, Neudörfl JM, Kühne R, Schmalz H-G (2011) Exercises in pyrrolidine chemistry: Gram scale synthesis of a Pro-Pro dipeptide mimetic with a polyproline type II helix conformation. *Chemistry* 17(43):12037–12044.
26. Grubbs RH, Chang S (1998) Recent advances in olefin metathesis and its application in organic synthesis. *Tetrahedron* 54(18):4413–4450.
27. Huy P, Neudörfl JM, Schmalz H-G (2011) A practical synthesis of trans-3-substituted proline derivatives through 1,4-addition. *Org Lett* 13(2):216–219.
28. Bittermann H, Gmeiner P (2006) Chirospecific synthesis of spirocyclic beta-lactams and their characterization as potent type II beta-turn inducing peptide mimetics. *J Org Chem* 71(1):97–102.
29. Kazmaier U, Mues H, Krebs A (2002) Asymmetric chelated Claisen rearrangements in the presence of chiral ligands: Scope and limitations. *Chemistry* 8(8):1850–1855.
30. Dinkel H, et al. (2014) The eukaryotic linear motif resource ELM: 10 years and counting. *Nucleic Acids Res* 42(Database issue):D259–D266.
31. Prehoda KE, Lee DJ, Lim WA (1999) Structure of the enabled/VASP homology 1 domain-peptide complex: A key component in the spatial control of actin assembly. *Cell* 97(4):471–480.
32. Bae YH, et al. (2010) Profilin1 regulates PI(3,4)P2 and lamellipodin accumulation at the leading edge thus influencing motility of MDA-MB-231 cells. *Proc Natl Acad Sci USA* 107(50):21547–21552.
33. Kuntz ID, Chen K, Sharp KA, Kollman PA (1999) The maximal affinity of ligands. *Proc Natl Acad Sci USA* 96(18):9997–10002.
34. Wells JA, McClendon CL (2007) Reaching for high-hanging fruit in drug discovery at protein-protein interfaces. *Nature* 450(7172):1001–1009.